

Two-photon imaging of soliton dynamics

Łukasz A. Sterczewski^{1,*}, and Jarosław Sotor¹

¹Faculty of Electronics, Photonics and Microsystems, Wrocław University of Science and Technology, Wyb. Wyspińskiego 27, 50-370 Wrocław, Poland

*e-mail: lukasz.sterczewski@pwr.edu.pl

Optical solitary waves (solitons) that interact in a nonlinear system can bind and form a structure similar to a molecule. The rich dynamics of this process have created a demand for rapid spectral characterization to deepen the understanding of soliton physics with many practical implications. Here, we demonstrate stroboscopic, two-photon imaging of soliton molecules (SM) with completely unsynchronized lasers, where the wavelength and bandwidth constraints are considerably eased compared to conventional imaging techniques. Two-photon detection enables the probe and tested oscillator to operate at completely different wavelengths, which permits mature near-infrared laser technology to be leveraged for rapid SM studies of emerging long-wavelength laser sources. As a demonstration, using a 1550 nm probe laser we image the behavior of soliton singlets across the 1800–2100 nm range, and capture the rich dynamics of evolving multiatomic SM. This technique may prove to be an essential, easy-to-implement diagnostic tool for detecting the presence of loosely-bound SM, which often remain unnoticed due to instrumental resolution or bandwidth limitations.

Since the discovery in hydrodynamic systems¹, solitary waves also known as solitons have expanded into diverse areas of science due to the unique way they analogize matter and waves. Arguably, a significant fraction of soliton research has been centered around nonlinear optical systems such as fibers² or microcavity resonators^{3,4}. This is because optical solitons do not spread out during propagation and exhibit robustness against perturbations; therefore they frame the core concept in optical pulse generation. Solitons also have the striking ability to form a stable bond between pairs or groups referred to as SMs^{5,6}. The binding force^{7,8} depends on the atomic spacing τ (temporal separation, TS), while the intramolecular phase $\Delta\varphi$ mostly governs the attraction/repulsion effect. Even more sophisticated physical systems like molecular complexes⁹ or molecular crystals¹⁰ can form via SM collisions. Despite advances in mathematical modeling¹¹, the understanding of these complex inter-soliton interactions still appears to be in infancy.

The rich landscape of nonlinear dynamics and numerous analogies to condensed-matter physics fuel intensive research in this field with much focus on studying the evolution dynamics and transient behavior of SM formation^{12,13}. It stems from the SM application potential to

optical memories, buffers¹⁴, or telecommunication to surpass the limitation of classical binary coding schemes^{15,16}. In such scenarios, one would like to tailor the SM spacing and phase on demand^{17,18,19,20} rather than rely on its uncontrolled organization, which necessitates a thorough characterization of transient short-lived SM states.

SM characterization techniques differ significantly in obtainable scan rates. Time-averaged (second-scale, Hz-rate) SM studies are performed with a first-order intensity autocorrelator (IAC) along with an optical spectrum analyzer (OSA)²¹, which are suitable mostly for steady-state phenomena like stable, tightly-bound SM. The highest scan rates (shot-to-shot, sub-GHz) are offered by the celebrated Dispersive Fourier Transformation (DFT) technique^{22,23}, which temporally stretches a laser pulse in a linear dispersive medium (such as optical fiber) to map the time domain to the frequency domain on a pulse-by-pulse basis^{12,13,24,18,25}. Unfortunately, beyond the 1–2 μm window, fiber losses may render this technique impractical. Also the spectral resolution of the two techniques (typically $\sim\text{GHz}$) may be insufficient to probe loosely-bound SMs (TS on the order of ns). A much simpler variant of this method – direct analysis of laser pulses on an oscilloscope without dispersive stretching – completely ignores the molecular phase and fails to resolve solitons spaced by ps due to electrical bandwidth limitations.

To fill a niche between the two timescales, recent works have proposed to adapt the phase-sensitive electric field cross-correlation (EFXC) technique²⁶ often referred to as coherent optical sampling²⁷ or dual-comb spectroscopy (DCS)²⁸ for imaging the dynamics of solitons in microresonators^{3,4}. However, high scan rates with EFXC are obtainable only with multi-GHz repetition-rate sources. In the case of fiber laser cavities, which constitute a majority of SM generators, the aliasing (Nyquist) limitation strongly constraints the observable optical bandwidth due to sources' low, MHz repetition rates, and restricts frame rates to the 10's–100's of Hz range. The need for phase locking between the lasers also adds a layer of complexity. The greatest difficulty, however, results from the need of a second, spectrally-matched laser, which may be impractical to implement at exotic wavelengths.

To bypass these limitations and unlock the kHz- to sub-MHz rate imaging potential, in this Article we adapt the non-interferometric intensity cross-correlation (IXC) technique²⁹ to the problem of dynamic soliton imaging.

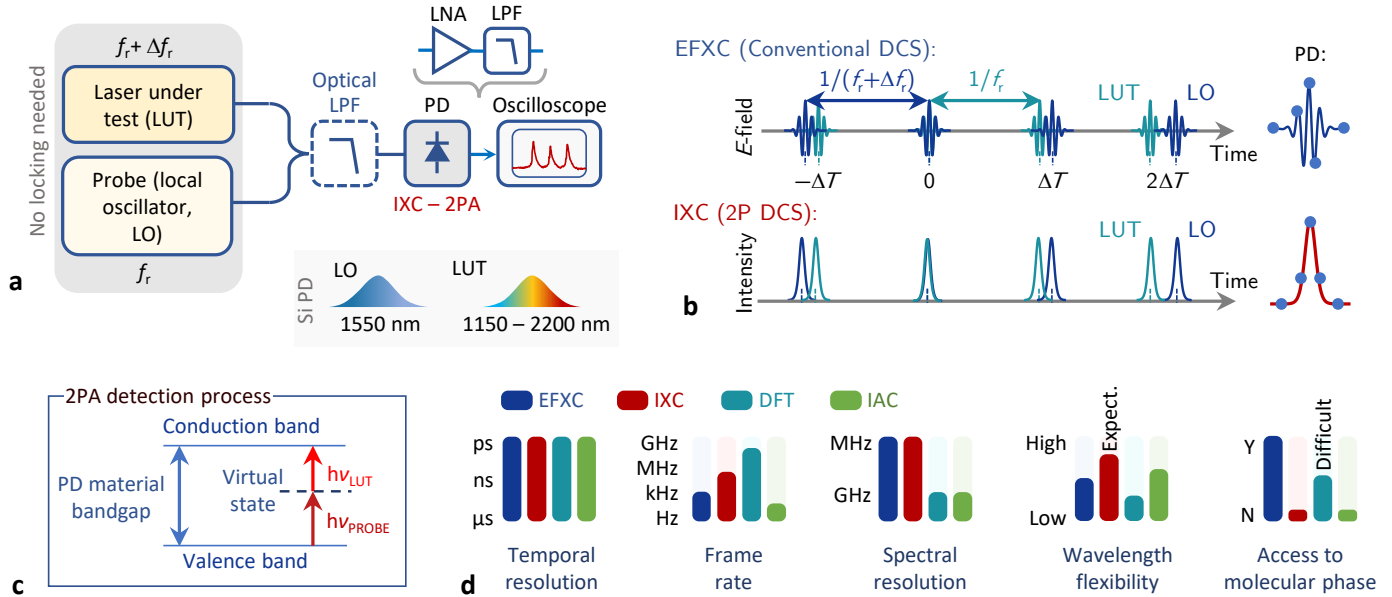


Figure 1 – Principles and experimental realization. **a** Conceptual schematic showing the laser under test (LUT) combined with a probe. After the long-pass-filtered (LPF) optical signal is measured on a photodetector (PD), a low-noise amplifier (LNA) followed by a low-pass filter (LPF) are used for signal conditioning prior to sampling by an oscilloscope. **b** Comparison of sampling in the EFXC, and IXC. The lag increases linearly from pulse-pair to pulse-air to produce EFXC and IXC signals. **c** Energy diagram of the 2PA detection process. **d** Chart-style comparison of existing SM characterization techniques in conventional realizations with the IXC technique.

Two-photon dual-comb IXC (or simply IXC throughout the rest of the text) probes SM dynamics with eased restrictions on the laser design, operation wavelength and stability. Instead of nonlinear crystals^{30,31} that require optical phase matching, the imaging technique builds on the two-photon detection ranging concept by Wright et al.³². Unlike EXFC, the IXC technique lifts the requirements of spectral overlap and phase lock between the two lasers: a pair of free-running sources with different wavelengths and offset repetition rates can be used instead. Only the probe and LUT photon energies must add to satisfy the 2-photon-absorption (2PA) detection criterion, which grants access to probing lasers in emerging spectral regions. Such an implementation of IXC may also extend the wavelength capabilities of techniques that retrieve the pulse temporal intensity profile (not just IAC) like FROG³³ or SPIDER³⁴, or speed of wavelength-agile cross-correlation FROG (XFROG)³⁵. If that of the probe pulse in IXC is characterized and known, the tested pulse profile one can be retrieved via deconvolution²⁹.

Results and discussion

Two-photon intensity cross-correlation. To image the SM behavior in an exemplary laser-under-test (LUT) cavity, we have probed it by a second mode-locked probe laser (referred to as a local oscillator, LO). On average, the lasers had tens of mW of optical powers and offered sub-ps pulse widths. The experimental setup is shown in Fig. 1a. Both sources were combined with a fiber coupler to jointly illuminate a commercial bias-free Si pho-

todiodode (PD, Thorlabs FDS02), which exhibits a 2PA response above ~ 1100 nm. To prevent one-photon absorption from occurring (i. e. due to residual above-bandgap pump or spurious light generated via nonlinear frequency conversion), we have incorporated a fiber long-pass filter (LPF) before the PD. The LUT repetition rate was $f_{r,1} \approx 100.04$ MHz, while the probe laser with $f_{r,2} = f_{r,1} + \Delta f_r$ was equipped with a tunable delay line to vary the cavity length and hence adjust the repetition rate difference Δf_r governing the IXC scan rate. The basic principle of the the IXC technique (Fig. 1b) resembles conventional DCS (EFXC), where a time lag of $\Delta T \approx \Delta f_r / f_r^2$ that linearly increases from pulse pair to pulse pair³⁶ stroboscopically samples the waveform over optical delays between 0 and $1/f_r$. In the case of dual-comb interferometry, measured is the phase-sensitive E -field cross-correlation also known as the interferogram (IGM), which relates the effective (ps/fs), and laboratory time (μ s/ns) time scales by the temporal magnification factor (TMF) $m = f_r / \Delta f_r$. However, the Nyquist frequency located at $f_r/2$ sets a limit on the maximum probed optical bandwidth $\Delta\nu$ expressed as $\Delta f_r \leq f_r^2 / 2\Delta\nu$, above which the probed IGM is badly distorted. Here, the full -20 dB bandwidth $\Delta\nu = 7.5$ THz (60 nm) can be probed with EFXC at rates $\Delta f_r \leq 670$ Hz. In IXC, the sampling process remains the same, however, the interaction relies on multiplying the combs' E -field intensities²⁹ $I_{1,2}(t) = |E_{1,2}(t)|^2$. The measured quantity is simply the intensity cross-correlation (\star): $\langle I_1(t)I_2(t + \tau) \rangle = \int_{-\infty}^{+\infty} I_1(t)I_2(t + \tau) dt = I_1(t) \star I_2(t)$, where τ represents the lag scanned by the asynchronous interaction. As

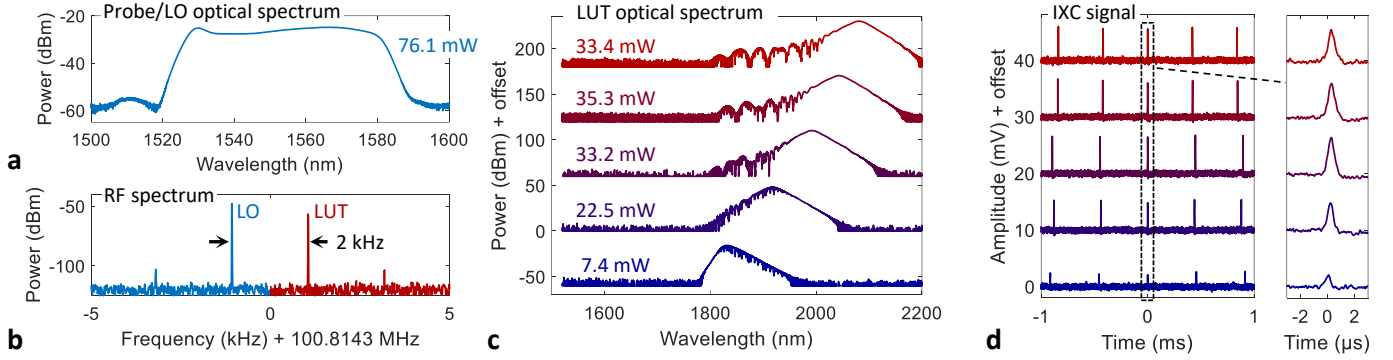


Figure 2 – Intensity cross-correlation between combs operating in different spectral regions. **a** Optical spectrum of the probe/LO laser. After amplification, the optical power is 76.1 mW. **b** Radio-frequency beat notes of the two combs detected by the Si detector when the LUT operates at 2100 nm. **c** Tunable optical spectra of the LUT due to the soliton self-frequency shift (SSF) process. **d** IXC signal measured with an oscilloscope for LUT spectra corresponding to those in panel (c).

will be shown later, the bandwidth limitations of IXC are not as strict as in EFXC, and can be exceeded multiple times the conventional limit.

Background-free 2PA in the semiconductor photodetector (Fig. 1c) produces a squared-intensity electrical response when a pair of photons with energies between half the bandgap and the bandgap reaches its surface (ideally tightly focused). The low efficiency of this $\chi^{(3)}$ process implies that only high peak powers (when two pulses temporally overlap) are detected. A major advantage is that the 2PA detection process does not require a polarization or wavelength match. Therefore, as long as the comb’s photon energies fall into a suitable range, an IXC signal can be produced. Once converted into the electrical domain, the signal should be conditioned by a low-noise amplifier (LNA), and a low-pass-filter (LPF) with $f_r/2$ cut-off to isolate the cross-correlation signal from the laser pulse trains prior to sampling by an oscilloscope. For a more detailed mathematical description of the IXC technique, please see Methods.

Weak wavelength constraints of IXC. The unique feature of IXC is its wavelength agility. To experimentally prove it, we employed a 1550 nm laser (Fig. 2a) to probe another longer-wavelength oscillator emitting pulses in the 1800–2100 nm range (Fig. 2b,c). For clarity of the demonstration, both sources were operated in the soliton singlet state, which yielded a clean IXC peak when the pulses coincided (Fig. 2d). This repeats periodically every $1/\Delta f_r$ seconds here equal to $(2 \text{ kHz})^{-1} = 500 \text{ ms}$, and produces a profile corresponding to the intensity cross-correlation between the pulses (see Methods for mathematical details). We would like to emphasize here the applicability of the technique to other spectral regions beyond the near-infrared. Provided a suitable two-photon detector (i.e. InGaAs or other semiconductor structures), it will be possible to employ technologically-mature thulium or holmium lasers and amplifiers to probe weaker mid-infrared oscillators. This is because the high-power probe/LO laser

can provide detection gain for weaker mW-class sources to produce a sufficiently strong IXC signal.

Scan rates and temporal resolution. With IXC, imaging SM dynamics over large optical bandwidths at high frame rates is possible beyond the aliasing limit of dual-comb interferometry, albeit at the expense of lowered temporal resolution. This counter-intuitive ability results from the practical condition that slightly chirped (non-transform-limited) pulses experience enhanced temporal overlap which broadens IXC features³². Since they occupy a smaller RF bandwidth, the aliasing constraints are relaxed (see Methods for more details). This feature enables us to directly illuminate the PD with broadband lasers without the need for narrow optical band-pass filtering, which complicates conventional EFXC.

Since the ultimate goal is almost always high imaging speed to fully capture the SM evolution trajectory, when comparing different SM diagnostic techniques one should consider the number of cavity round-trips required to produce a single frame rather than absolute time units. For instance, MHz scan rates obtained in imaging GHz-level f_r microcavities^{3,4} require 10^3 round-trips per frame. In relative terms, imaging $f_r = 100 \text{ MHz}$ fiber laser cavities with $\Delta f_r = 100 \text{ kHz}$ frame rates is equivalent. This is what can be obtained using the IXC technique even for low f_r cavities, as shown in Fig. 3a.

In this context, worth studying is also a single-frame IXC temporal resolution limit, which governs the ability to identify tightly-bound SM atoms and sets another limit on Δf_r . The requirement to low-pass filter the electrical IXC signal at $f_r/2$ implies that only features spaced in laboratory time by $\delta t_{\text{lab}} > 2/f_r$ can be resolved, which given the TMF, yields an effective temporal resolution limit $\delta t_{\text{eff}} = 2\Delta T = 2\Delta f_r/f_r^2$. For a $f_r = 100 \text{ MHz}$ laser, this corresponds to $\delta t_{\text{eff}} = 2 \text{ ps}$ for $\Delta f_r = 10 \text{ kHz}$. It is therefore clear that the IXC technique is favored for probing larger temporal separations with high frame rates (where DFT struggles due to bandwidth and resolution

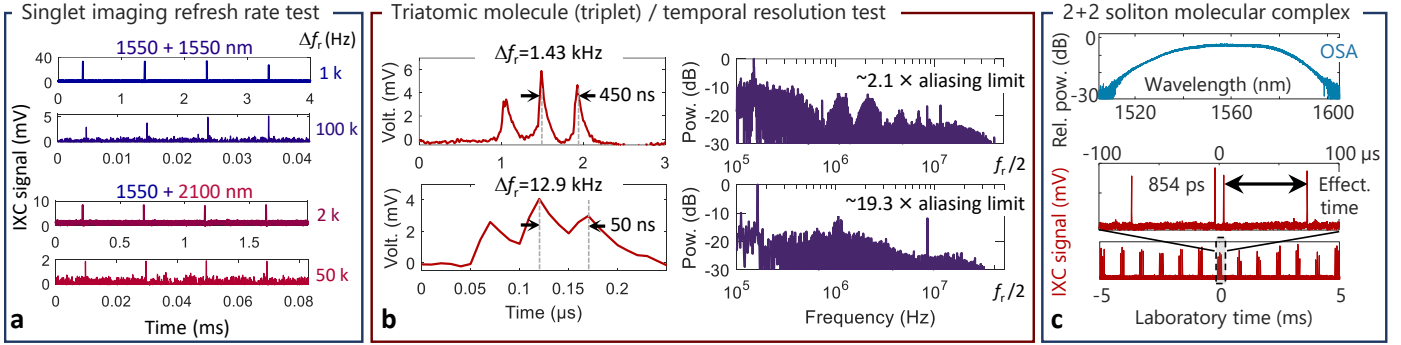


Figure 3 – Scan rate and temporal resolution test. **a** Agility in obtainable scan rates for lasers operating at the same, and different wavelengths. The lowered signal level at higher rates results from the lower number of coincidence/overlap events when a single IXC trace is produced. **b** Temporal resolution test that shows operation above the aliasing limit. A soliton triplet (triatomic molecule) is imaged. Even exceeding the aliasing limit almost 20 times still yields resolved pulses. Shown also is the power spectrum of the IXC signal, which is mostly concentrated in the low-frequency region rather than close to the Nyquist frequency $f_r/2$. **c** 2+2 soliton molecular complex (SMC) probed by the IXC technique. The soliton pairs are separated by 88 ps, while the atom separation is 0.854 ns, which practically requires sub-GHz spectral resolutions to detect its presence. Such features are not resolved by a 50 pm (~ 6 GHz) resolution optical spectrum analyzer (OSA).

limitations), while tightly-bound SMs entail scanning at lower rates. An experimental verification of these derivations is shown in Fig. 3b. A triatomic SM with a 6.45 ps TS has clearly resolvable atoms even when exceeding the aliasing limit ~ 20.8 times. In the laboratory time scale, the atoms are spaced by ~ 50 ns, which is $2.5\times$ the resolution limit ($\delta t_{\text{eff}} = 2.58$ ps). Obviously, distinguishing features in the near-resolution-limit regime may be difficult, because the significant fall time of the IXC signal due to the LPF lowers the peak contrast.

IXC for laser diagnostics. Notably, IXC can serve as a practical laboratory diagnostic tool to detect the presence of multiple pulses in a laser cavity. The 0 – f_r delay scan range with a corresponding f_r resolution limit analogous to a mechanical interferometer displacement on the order of meters for fiber laser cavities, is far beyond most DFT implementations, high-resolution OSAs, and even long-range autocorrelators. In many biomedical imaging applications like two-photon fluorescence³⁷, pulse parameters such as peak power are derived solely from short-range (< 50 ps) intensity autocorrelation traces. If loosely-bound SMs form inside the cavity (and hence there is more than one pulse per round-trip), these assumptions may be completely invalid. IXC diagnostics addresses these challenges, as shown in Fig. 3c. Interestingly, probed is not a simple di- or tetratomic SM, but a recently discovered pair of bound pulses referred to as a 2+2 soliton molecular complex (SMC)⁹ with distinct intra- and inter-molecular bonds. The intra-molecular TS is 854 ps, while the inter-molecular TS is 88 ps, which are in opposite ratios compared to those observed in ref.⁹. Resolving such widely-spaced pulses would practically require a sub-GHz resolution, which is rarely possible with typical OSAs or IAC.

Two-photon imaging of SM dynamics. To demonstrate the extended-time IXC imaging capabilities, we vi-

sualize the evolution of SMs produced by a mode-locked fiber laser with $f_r = 100.04$ MHz repetition rate covering $\Delta\nu > 60$ nm of -20 dB optical bandwidth centered at ~ 1550 nm. High pump levels (> 500 mW) lead to the excitation of tightly-bound tri- and tetratomic SMs, of which only the first was indefinitely stable. The fine intramolecular motion of these SM states was probed by IXC with 270 fs, and 230 fs temporal resolution (defined by $f_r/2$) in the soliton triplet and quadruplet case, respectively. Figure 4a shows the IXC signal (intensity cross-correlogram) sampled by a 12-bit oscilloscope. Subsequent zoomed panels reveal a sequence repeating with $\Delta f_r = 1.35$ kHz, which appears as three isolated pulses spaced by 500 ns. In this experiment, the probe laser (Fig. 2a) was completely unsynchronized with the LUT, as Hz-level Δf_r stability on a second timescale yielded a relative timing uncertainty in the 10^{-3} range. A waterfall-type sequence of frames sampled Δf_r per second yielded an IXC image, where the vertical (y -axis) was scaled according to the TMF, analogous to applying a co-moving time frame^{12,3}.

In the triatomic molecule case (Fig. 4b), one can observe weak intermolecular motions from the nominal 6 ps spacing. Nevertheless, the trajectories drawn by the atoms are clear and saturated, as zoomed in Fig. 4c. This picture finds confirmation in the optical spectrum measured with an OSA (Fig. 4d), which displays a regular modulation pattern with a 1.2–1.3 nm (~ 161 GHz) period. The simultaneously measured radio frequency (RF) spectrum (Fig. 4e) does not show any anomalies.

In contrast, the unstable tetratomic molecule (Fig. 4f) exhibits rich nonlinear dynamics reminiscent of mode competition in semiconductor lasers. Almost never do all four pulses have comparable intensities. Instead, whenever some pulses become stronger, others weaken, as plotted in zoomed-panel Fig. 4g. Notably, the TS of

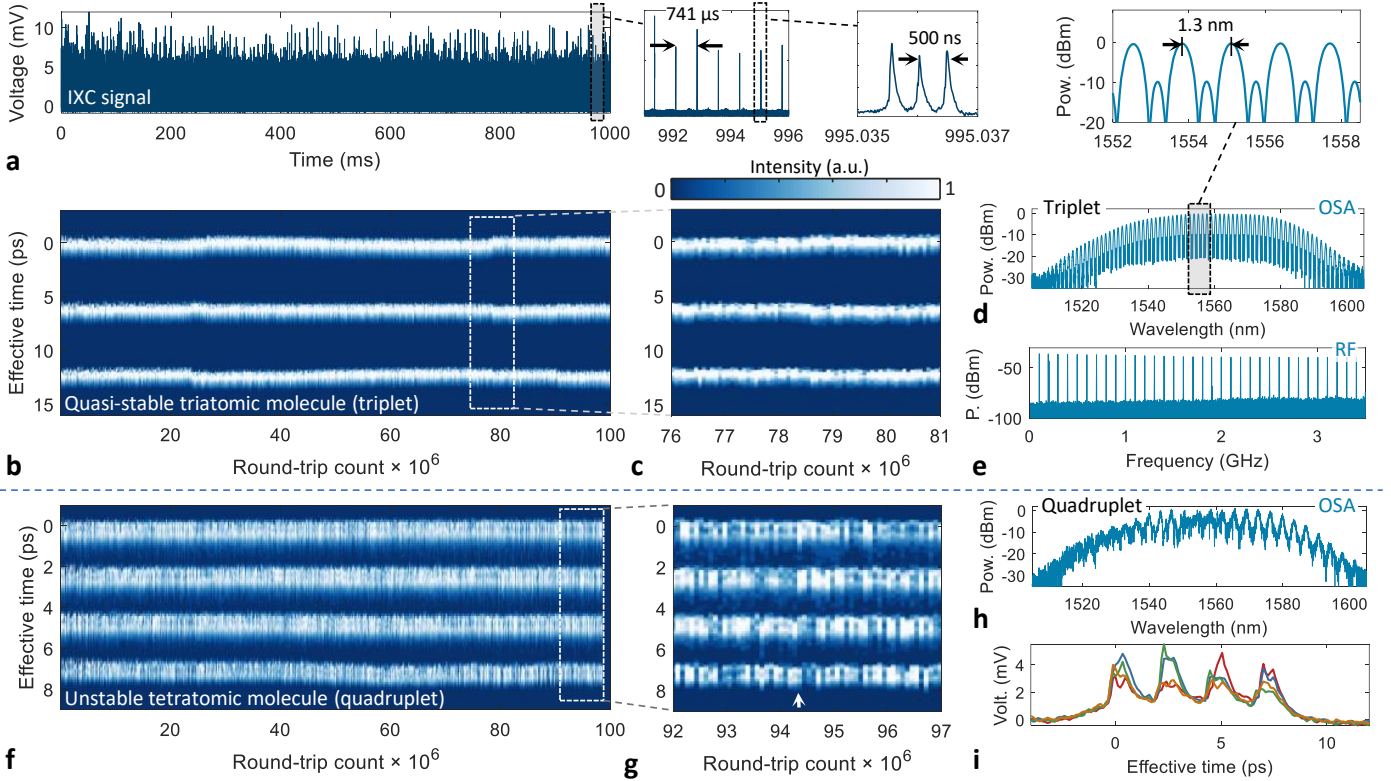


Figure 4 – IXC imaging of SM dynamics in a quasi-stable triatomic (a–e) and unstable tetratomic state (f–i). **a** Amplified IXC signal acquired over 1 second, when the LUT was operated in the quasi-stable triatomic SM state. Subsequent panels show zoomed portions of the signal revealing the existence of 3 isolated pulses. **b** Imaging soliton molecule trajectory, where slight, sub-ps variations of the TS are visible. An analogously-long DFT waveform (1 s) measured using a 5 GHz 8-bit oscilloscope would have a size of ~ 10 GB, while the 12-bit 50 MHz bandwidth IXC dataset occupies 360 MB. Segmented acquisition in a narrower temporal span (to several microseconds each frame) may lower the size to ~ 1 MB. **c** Zoom of (b), which shows nearly-constant peak intensities. **d** Optical spectrum with a strong 1.2–1.3-nm-period modulation (~ 161 GHz) due to the presence of three bound pulses. **e** Radio-frequency (RF) spectrum measured by an InGaAs photodetector. It is nearly the same for panels (f–i). **f** IXC image of an unstable tetratomic molecule (quadruplet), with competition-like behavior between the pulses. **g** Zoom of the framed part showing the rapidly oscillating intensities of the SM pulses, in stark contrast to (b). **h** Optical spectrum acquired in parallel with IXC, which shows a dynamic evolution of the fringe contrast and noise-like envelope. **i** 4 slices of the IXC image in the region pointed by arrow in (g).

~ 2.3 ps barely fluctuates except for minor drift of the 4-th atom above $60 \cdot 10^6$ round-trips. This noisy behavior finds confirmation in the optical spectrum (Fig. 4h), which lacks a regular modulation pattern and cannot be used to explain the laser state by itself. Throughout the duration of the scan, the soliton quadruplet was rapidly evolving, which corrupted the fringe contrast in the optical spectrum. Example four consecutive IXC frames are given in Fig. 4i.

Microsecond-time imaging of soliton-rain-like phenomena. To demonstrate the rapid temporal dynamics capabilities of IXC imaging and agility in obtainable frame rate, we have probed a soliton-rain-like event³⁸ with $\Delta f_r = 83$ kHz yielding a horizontal resolution of ~ 1200 cavity round-trips (12 μ s). Increased laser cavity losses (due to fiber bending) accompanied by high pump powers give rise to a significant quasi-continuous-wave (CW) component in the optical spectrum, which in turn mediates long-range soliton interactions. This laser state corresponds to a weakly mode-locked regime when low-intensity

light filtering is not efficient to prevent multiple unlocked pulses from existing. Four IXC frames shown in Fig. 5a display a quasi-repeating yet evolving pattern with characteristic intensive regions (i. e. around 40 μ s) referred to as the condensed phase surrounded by a soliton flow part. The soliton rain process resembles rain droplet formation from a vapor cloud, where spontaneously created "rain droplets" move toward the condensed phase like they were falling into the sea to next evaporate and start the process again³⁸. Magnification of one of the frames reveals that multiple pulses spaced by approximately 90 ns exist during a round-trip. Like before, even $\sim 124\times$ above the aliasing limit, the IXC signal, and its frequency spectrum (Fig. 5b) look clean and undistorted. The quasi-harmonic IXC spectrum has a regular structure with broad peaks, which reflect the soliton position timing jitter. The peak locations are multiples of ~ 11 MHz related to the ~ 90 ns laboratory time soliton spacing (75 ps effective). Except for the aforementioned CW component, the optical spectrum (Fig. 5c) does not have any special features. The RF

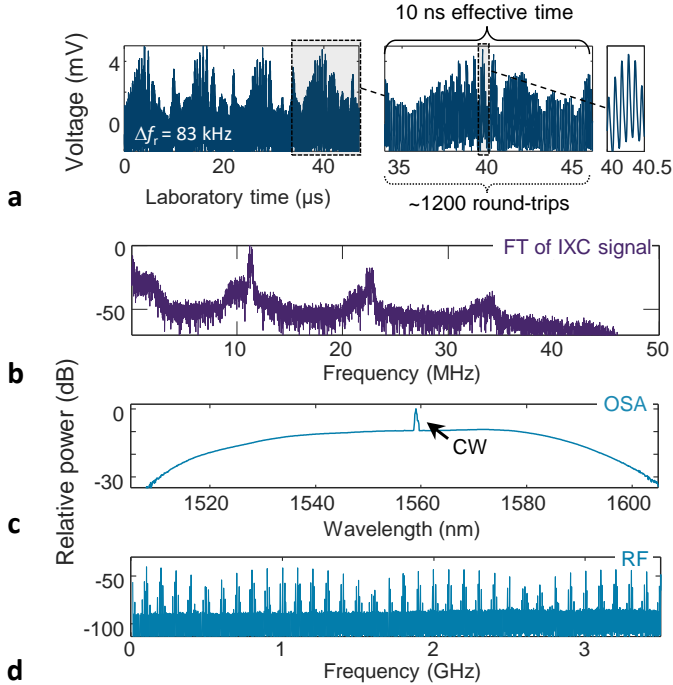


Figure 5 – Soliton-rain-like-event mediated by a strong CW component. **a** IXC signal with $\Delta f_r = 83$ kHz scan rate, which is $\sim 123\times$ above the aliasing limit. Zoomed panels resolve individual pulses. **b** Power spectrum of the IXC signal via the Fourier transform (FT). **c** Optical spectrum with a continuous-wave (CW) component. **d** Strongly modulated RF spectrum, which reflects the complex dynamics of this laser state at extended timescales.

spectrum (Fig. 5d), in contrast, is strongly modulated with multiple sidebands, which is a signature of the rich soliton rain dynamics at extended time scales. It is clear that IXC directly images the temporal SM dynamics, as opposed to providing time-averaged measurements obtained using swept optical- or RF spectrum analyzers.

Conclusions and outlook

Imaging of SM dynamics in a fiber laser cavity using a two-photon modality of DCS has been demonstrated. To achieve the high frame rates needed to capture the intramolecular motion over large optical bandwidths, two-photon IXC is measured. The technique enables one to surpass the conventional aliasing limit of DCS, while simultaneously offering eased requirements on the optical setup and large wavelength flexibility. We show that a mature 1550 nm mode-locked laser can probe another free-running mode-locked source operating at the same wavelength, or in the 1800–2100 nm wavelength range. This agility may be instrumental for diagnosing novel, mid-infrared mode-locked lasers³⁹, where the availability of optical components such as fibers or amplifiers for DFT is scarce. Even single-cavity dual-wavelength oscillators with asynchronous pulses that do not spectral overlap⁴⁰ can be directly studied for SM merely by illuminating a

commercially-available two-photon photodiode.

IXC imaging of stable tri-atomic, and an unstable tetratomic SMs at kHz rates enables us to identify that the tetratomic molecule exhibits dynamic pulse competition effects, which corrupt the optical spectrum but are not directly visible in the RF spectrum. Probing this phenomenon at such rates and resolution would not have been possible using a swept OSA, conventional IAC or non-DFT-enhanced oscilloscope. Next, increasing the repetition rate difference between the lasers to almost 100 kHz grants us access to high-rate imaging of a soliton rain, albeit at the expense of temporal resolution.

We believe that the IXC imaging technique fills the important niche between slow, time-averaged measurements performed by IAC or OSAs, and pulse-by-pulse diagnostics offered by DFT or direct pulse digitization by a high-bandwidth oscilloscope. From a practical standpoint, IXC is the perfect candidate for an easy-to-implement diagnostic tool in photonic laboratories to probe the existence of previously unseen loosely bound molecules due to the delay-resolution limit of autocorrelators or limited speed of oscilloscopes and photodiodes employed in DFT. For IXC-enabled laser diagnostics of sources with arbitrary repetition rates, we envision the application of amplified electro-optic (EOM) combs to serve as repetition-rate-agile probe sources.

Another strength of the IXC imaging technique lies in that it simplifies long-term SM studies while maintaining high scan rates. Because of the IXC signal’s typically low duty cycle, segmented frame acquisition in a narrower effective time span may drastically reduce the amount of recorded data by orders of magnitude. This may prove to be difficult for competing spectral-domain techniques like DFT. Greatly benefit from IXC-enabled studies may also supercontinuum sources, whose large bandwidths make EFXC studies possible only at very low rates, while fiber parameters for implementing shot-to-shot DFT drastically change over the octave spans of supercontinua. Particularly such application scenarios call for developing two-photon detectors with higher optical nonlinearities to enable operation with lower average powers and broader optical pulses.

Methods

Intensity cross-correlation. Asynchronous interaction between optical pulses on a photodetector that exhibits a square-law response with respect to intensity $I(t) = |E(t)|^2$ rather than E -field ($P(t) \sim I(t)^2$) produces an intensity cross-correlation (IXC) signal. The instantaneous optical power seen by the two-photon-absorption (2PA) detector is

$$P_{2PA}(t) = I_1^2(t) + I_1(t)I_2(t) + I_2^2(t). \quad (1)$$

Extended timescale averaging / integration yields a photodetector voltage

$$V \sim \langle P_{2PA}(t) \rangle = \frac{1}{2} \left(\int_{-\infty}^{\infty} I_1(t)^2 dt + \int_{-\infty}^{\infty} I_2(t)^2 dt + \int_{-\infty}^{\infty} I_1(t)I_2(t) dt \right). \quad (2)$$

Adding a variable time delay τ (lag) between I_1 and I_2 makes this signal more informative. The photodetector response now reads:

$$V(\tau) \sim \langle P_{2PA}(t, \tau) \rangle = \frac{1}{2} \left(\langle I_1^2(t) \rangle + \langle I_2^2(t + \tau) \rangle + \langle I_1(t)I_2(t + \tau) \rangle \right). \quad (3)$$

One recognizes the intensity cross-correlation in the last term in addition to near-DC time-averaged squared pulse energies $I_{1,2}^2(t)$. This is the relevant term that survives in the electrical signal after low-pass filtering at $f_r/2$:

$$\langle I_1(t)I_2(t + \tau) \rangle = \int_{-\infty}^{\infty} I_1(t)I_2(t + \tau) dt = I_1(t) \star I_2(t). \quad (4)$$

In its most straightforward realization, measuring the IXC requires a mechanical stage that introduces lag $\tau = 2\Delta L/c$ when moved by ΔL (thus bounding the domain of integration of the improper cross-correlation integral). Unfortunately, the mechanical nature of the scan makes it obviously slow and suffers from resolution limitations analogous to Fourier Transform Spectroscopy (FTS). High resolution studies simply require long optical displacements. These limitations can be circumvented if one restricts the class of sources under study to pulsed lasers, or more generally sources with a well-defined repetition rate f_r . For such, an elegant way to introduce a variable lag is provided by means of dual-comb spectroscopy (DCS)^{41,28} or equivalently asynchronous optical sampling (ASOPS)⁴². A second repetition-rate-mismatched source ($f_r + \Delta f_r$) provides a linearly varying (although discretized) lag that increases by $\Delta T \approx \Delta f_r/f_r^2$ from pulse pair to pulse pair³⁶ (Fig. 1b). This periodically samples (cross-correlates) the waveform over optical delays between 0 and $1/f_r$ thus producing an intensity cross-correlogram stretched in time by $m = f_r/\Delta f_r$. The process repeats itself at a $1/\Delta f_r$ rate, which ranges between nanoseconds to sub-seconds.

Comparison with EFXC: Due to differences between IXC and conventional EFXC/DCS, we provide Table 1 that summarizes the prerequisites and limitations of the two techniques. This comparison is valid for a laser repetition frequency of $f_r = 100$ MHz or lower. Higher repetition rates (GHz) imply lower peak intensities, which necessitates more average power for IXC detection.

Violation of the Nyquist criterion: In the weakly-chirped regime, measuring the IXC high above the aliasing limit requires one to ensure an integer $k = f_r/\Delta f_r$ ratio to avoid signal scalloping, Vernier-like filtering effects. Because only discrete effective time intervals spaced by $1/(kf_r)$ are probed, features far away from this temporal grid may not be sampled, and hence overlooked. On the other hand, non-integer k ratios offer enhanced temporal resolution due to scanning all possible LUT-probe relative delays like in a sampling oscilloscope. That said, acquiring such high-resolution scans takes multiple Δf_r periods. Clearly, different trade-offs must be taken into account when violating the aliasing limit.

Dual-wavelength IXC experiment: To obtain tunable pulses at longer wavelengths, we employ the soliton self-frequency shift effect in a highly nonlinear fiber. The experimental setup follows ref.⁴³. To ensure that only the long-wave part of the spectrum interacts with the probe laser, we employ a cascade of wavelength domain multiplexing (WDM) filters/couplers to reject the original non-shifted pulse components (as seen in Fig. 2c) by at least 40 dB.

Importance of the pulse amplifier: Because the intensity cross-

correlogram is of pulsed unipolar nature, amplifying such a signal requires an amplifier with almost contradictory requirements: low noise figure, broad electrical bandwidth, and a low frequency limit extending almost to DC. Empirically, we found that the low frequency limit of 10 kHz is sufficient, while typical radio-frequency amplifiers operating above 1 MHz severely distort the IXC signal due to their high-pass properties. In all experiments here, we used a 2 GHz, 40 dB HSA-X-2-40 RF amplifier (Femto, Germany), which meets the aforementioned requirements. All IXC signal levels (in the mV range) indicated in this paper refer to the nominal signal from the unbiased Si photodiode after the 40 dB amplifier (100 V/V voltage gain).

References

- Russell, J. S. *Report on Waves: Report of the Fourteenth Meeting of the British Association for the Advancement of Science* (John Murray, 1845).
- Mollenauer, L. F. & Stolen, R. H. The soliton laser. *Optics Letters* **9**, 13–15 (1984).
- Yi, X., Yang, Q.-F., Yang, K. Y. & Vahala, K. Imaging soliton dynamics in optical microcavities. *Nature Communications* **9**, 3565 (2018).
- Weng, W. *et al.* Heteronuclear soliton molecules in optical microresonators. *Nature Communications* **11**, 2402 (2020).
- Malomed, B. A. Bound solitons in the nonlinear Schroedinger–Ginzburg–Landau equation. *Physical Review A* **44**, 6954–6957 (1991).
- Stratmann, M., Pagel, T. & Mitschke, F. Experimental observation of temporal soliton molecules. *Physical Review Letters* **95**, 143902 (2005).
- Gordon, J. P. Interaction forces among solitons in optical fibers. *Optics Letters* **8**, 596–598 (1983).
- Mitschke, F. M. & Mollenauer, L. F. Experimental observation of interaction forces between solitons in optical fibers. *Optics Letters* **12**, 355 (1987).
- Wang, Z. Q., Nithyanandan, K., Coillet, A., Tchifo-Dinda, P. & Grellu, P. Optical soliton molecular complexes in a passively mode-locked fibre laser. *Nature Communications* **10**, 830 (2019).
- Cole, D. C., Lamb, E. S., Del’Haye, P., Diddams, S. A. & Papp, S. B. Soliton crystals in Kerr resonators. *Nature Photonics* **11**, 671–676 (2017).
- Dauxois, T. & Peyrard, M. *Physics of Solitons* (Cambridge University Press, 2006).
- Herink, G., Kurtz, F., Jalali, B., Solli, D. R. & Ropers, C. Real-time spectral interferometry probes the internal dynamics of femtosecond soliton molecules. *Science* **356**, 50–54 (2017).
- Liu, X., Yao, X. & Cui, Y. Real-Time Observation of the Buildup of Soliton Molecules. *Physical Review Letters* **121**, 023905 (2018).
- Boyd, R. W., Gauthier, D. J. & Gaeta, A. L. Applications of slow light in telecommunications. *Optics and Photonics News* **17**, 18–23 (2006).
- Akhmediev, N. N., Town, G. & Wabnitz, S. Soliton coding based on shape invariant interacting soliton packets: The three-soliton case. *Optics Communications* **104**, 385–390 (1994).
- Rohrman, P., Hause, A. & Mitschke, F. Solitons Beyond Binary: Possibility of Fibre-Optic Transmission of Two Bits per Clock Period. *Scientific Reports* **2**, 866 (2012).
- He, Y., Ling, J., Li, M. & Lin, Q. Perfect Soliton Crystals on Demand. *Laser & Photonics Reviews* **14**, 1900339 (2020).
- Kurtz, F., Ropers, C. & Herink, G. Resonant excitation and all-optical switching of femtosecond soliton molecules. *Nature Photonics* **14**, 9–13 (2020).
- Liu, S., Cui, Y., Karimi, E. & Malomed, B. A. On-demand harnessing of photonic soliton molecules. *Optica* **9**, 240 (2022).
- Nimmegern, L., Beckh, C., Kempf, H., Leitenstorfer, A. &

	EFXC	IXC
Response	Linear	Nonlinear (two-photon)
Interferometric	Yes	No
Polarization matching required	Yes	No [§]
Required average power	1–100 μ W	$\sim 1^*$ –100 mW
Required pulse-width	Arbitrary	\sim ps [¶] or lower
Spectral overlap	Required	No, only photon energies must add
Access to molecular phase	Yes	No
Lock between the lasers	Not needed for multiplexed cavities	Not needed
Aliasing problem	Yes, bandwidth $\Delta\nu \leq f_r^2/(2\Delta f_r)$	No [†] , but limited by the LUT dynamics

Table 1 – Comparison of dual-comb based techniques for imaging of SM dynamics and laser diagnostics. EFXC – electric field cross-correlation, IXC – intensity cross-correlation. [§]Avoiding polarization alignment between the two lasers prevents interferometric effects that would arise like in fringe-resolved IAC when operating at the same wavelength. ^{*}Photodetectors with higher nonlinear coefficients should grant access to probing pulsed lasers with 1 mW or lower average power. Currently, it is several mW. [¶]Longer pulses (dozens of ps) should also be detectable when a higher sensitivity 2PA photodetector is used. [†]Operation high above the aliasing limit requires a careful choice of Δf_r with respect to the pulse width.

- Herink, G. Soliton molecules in femtosecond fiber lasers: Universal binding mechanism and direct electronic control. *Optica* **8**, 1334 (2021).
21. Tang, D. Y., Man, W. S., Tam, H. Y. & Drummond, P. D. Observation of bound states of solitons in a passively mode-locked fiber laser. *Physical Review A* **64**, 033814 (2001).
 22. Tong, Y., Chan, L. & Tsang, H. Fibre dispersion or pulse spectrum measurement using a sampling oscilloscope. *Electronics Letters* **33**, 983–985 (1997).
 23. Goda, K. & Jalali, B. Dispersive Fourier transformation for fast continuous single-shot measurements. *Nature Photonics* **7**, 102–112 (2013).
 24. Luo, Y. *et al.* Real-time access to the coexistence of soliton singlets and molecules in an all-fiber laser. *Optics Letters* **44**, 4263 (2019).
 25. Zhao, K., Gao, C., Xiao, X. & Yang, C. Real-time collision dynamics of vector solitons in a fiber laser. *Photonics Research* **9**, 289 (2021).
 26. Ferdous, F., Leaird, D. E., Huang, C.-B. & Weiner, A. M. Dual-comb electric-field cross-correlation technique for optical arbitrary waveform characterization. *Optics Letters* **34**, 3875 (2009).
 27. Coddington, I., Swann, W. C. & Newbury, N. R. Coherent linear optical sampling at 15 bits of resolution. *Optics Letters* **34**, 2153 (2009).
 28. Coddington, I., Newbury, N. & Swann, W. Dual-comb spectroscopy. *Optica* **3**, 414 (2016).
 29. Nicholson, J. W., Jasapara, J., Rudolph, W., Omenetto, F. G. & Taylor, A. J. Full-field characterization of femtosecond pulses by spectrum and cross-correlation measurements. *Optics Letters* **24**, 1774 (1999).
 30. Zhang, H., Wei, H., Wu, X., Yang, H. & Li, Y. Absolute distance measurement by dual-comb nonlinear asynchronous optical sampling. *Optics Express* **22**, 6597 (2014).
 31. Han, S., Kim, Y.-J. & Kim, S.-W. Parallel determination of absolute distances to multiple targets by time-of-flight measurement using femtosecond light pulses. *Optics Express* **23**, 25874 (2015).
 32. Wright, H., Sun, J., McKendrick, D., Weston, N. & Reid, D. T. Two-photon dual-comb LiDAR. *Optics Express* **29**, 37037 (2021).
 33. Kane, D. J. & Trebino, R. Characterization of arbitrary femtosecond pulses using frequency-resolved optical gating. *IEEE Journal of Quantum Electronics* **29**, 571–579 (1993).
 34. Iaconis, C. & Walmsley, I. A. Spectral phase interferometry for direct electric-field reconstruction of ultrashort optical pulses. *Optics Letters* **23**, 792–794 (1998).
 35. Linden, S., Giessen, H. & Kuhl, J. XFROG – A new method for amplitude and phase characterization of weak ultrashort pulses. *Physica Status Solidi (b)* **206**, 119–124 (1998).
 36. Picqué, N. & Hänsch, T. W. Frequency comb spectroscopy. *Nature Photonics* **13**, 146–157 (2019).
 37. Boguslawski, J. *et al.* In vivo imaging of the human eye using a 2-photon-excited fluorescence scanning laser ophthalmoscope. *The Journal of Clinical Investigation* **132**, e154218 (2022).
 38. Chouli, S. & Grellu, P. Rains of solitons in a fiber laser. *Optics Express* **17**, 11776 (2009).
 39. Ma, J., Qin, Z., Xie, G., Qian, L. & Tang, D. Review of mid-infrared mode-locked laser sources in the 2.0 μ m–3.5 μ m spectral region. *Applied Physics Reviews* **6**, 021317 (2019).
 40. Liao, R. *et al.* Dual-comb generation from a single laser source: Principles and spectroscopic applications towards mid-IR—A review. *Journal of Physics: Photonics* **2**, 042006 (2020).
 41. Keilmann, F., Gohle, C. & Holzwarth, R. Time-domain mid-infrared frequency-comb spectrometer. *Optics Letters* **29**, 1542 (2004).
 42. Elzinga, P. A., Lytle, F. E., Jian, Y., King, G. B. & Laurendeau, N. M. Pump/probe spectroscopy by asynchronous optical sampling. *Applied Spectroscopy* **41**, 2–4 (1987).
 43. Soboń, G., Martynkien, T., Tarnowski, K., Mergo, P. & Sotor, J. Generation of sub-100 fs pulses tunable from 1700 to 2100 nm from a compact frequency-shifted Er-fiber laser. *Photonics Research* **5**, 151–155 (2017).

Acknowledgements

This project has received funding from the European Union’s Horizon 2020 research and innovation programme under the Marie Skłodowska-Curie grant agreement No 101027721. This work is supported by the use of National Laboratory for Photonics and Quantum Technologies (NPLQT) infrastructure, which is financed by the European Funds under the Smart Growth Operational Programme. Dr. Jakub Boguslawski at Wrocław University of Science and Technology, Poland is acknowledged for fruitful discussions on the importance of laser pulse diagnostics for nonlinear frequency conversion.

Author contributions

L.A.S., and J.S. conceived the idea. L.A.S. carried out the optical and electrical measurements, analyzed the data, and generated the figures. J. S. fabricated the mode-locked lasers. L.A.S and J.S. wrote the manuscript. J.S. coordinated the project.

Conflict of interest

The authors declare no conflict of interest.

Data availability statement

The data that support the plots within this paper and other findings of this study are available from the corresponding author upon reasonable request.